J Mater Sci (2022) 57:7035–7041

Energy materials

Lithium diffusion in lithium tantalate as measured by confocal Raman spectroscopy

Jacob M. Ivy[1] and Geoff L. Brennecka[1,*]

[1] George S Ansell Department of Metallurgical and Materials Engineering, Colorado School of Mines, Golden, CO, USA

Received: 12 October 2021
Accepted: 15 March 2022
Published online: 28 March 2022

ABSTRACT

A two-stage vapor transport equilibration (VTE) has been employed to mitigate lithium deficiency in single crystals of lithium tantalate, $LiTaO_3$. This work details a low-temperature vapor transport infiltration (VTI) anneal step that establishes a lithium-rich surface layer in the treated samples which annihilates the intrinsic point defect complexes of congruent $LiTaO_3$ while allowing depth and concentration profiles of the point defects to be measured via confocal Raman spectroscopy at different stages in the process. These data are then used to calculate diffusion coefficients for lithium in $LiTaO_3$, which range between 4.2×10^{-11} and 2.9×10^{-10} cm^2/s between 950 and 1100 °C. The lithium gradients are removed, and sample chemistry is equilibrated during a second, higher-temperature anneal in an ambient atmosphere and confirmed via additional Raman measurements. Temperature-dependent impedance spectroscopy data are also used to confirm the presence or absence of lithium gradients in these samples and show that lithiation of $LiTaO_3$ takes place at temperatures as low as 950 °C.

Introduction

Lithium tantalate ($LiTaO_3$) is a uniaxial ferroelectric commonly used in a variety of electro-optic, nonlinear-optic, photo-refractive, and acoustic devices. Typically, this material is produced as single crystals grown at the congruent melting composition of Li/Ta ≈ 0.94. The lithium deficiency is accommodated through a combination of lithium vacancies (V_{Li}') and charge compensating tantalum antisite defects ($Ta_{Li}^{\cdots\cdot}$) that cluster together below ~200 °C to form tetrahedra in which the central antisite ion is bordered by three vacancies in the nearest cation plane and an additional independent vacancy that lies along the *z*-axis [1–3]. These defect complexes have drastic effects on optical and ferroelectric properties including an increased saturated space charge field [4], increased susceptibility to photorefractive damage [5], an approximate two hundred-fold increase in coercive field [6, 7], and an ~100 °C decrease in Curie temperature over stoichiometric crystals [8, 9]. The

Handling Editor: Mark Bissett.

Address correspondence to E-mail: gbrennec@mines.edu

https://doi.org/10.1007/s10853-022-07105-y

changes in coercive field and Curie temperature in particular have been shown to be linearly related to the change in point defect concentration and are frequently used as rapid and effective methods to indirectly determine lithium stoichiometry in $LiTaO_3$ [9, 10]. The Raman spectrum of $LiTaO_3$ is also sensitive to Li stoichiometry, with Li deficiency causing peak broadening and the development of new Raman modes with increasing point defect concentration [11–13].

Avoidance of Li deficiency during growth is possible using a double-crucible Czochralski technique and a melt chemistry with significant lithium excess, but this approach suffers from significantly greater occurrences of stress cracking and inclusions than growth of the congruent composition [6, 8]. A post-growth technique known as vapor transport equilibration (VTE) increases the Li content in the specimen by annealing the crystal in a loosely enclosed system above a powder that evolves Li_2O vapor at high temperatures [9, 14]. VTE anneals conventionally occur at temperatures in excess of 1200 °C for $LiTaO_3$ and can last for a few hundred hours, depending upon crystal thickness [2, 15].

Despite the clear interest in restoring Li/Ta stoichiometry over the last thirty years, the authors could find only one quantitative report of Li diffusion in $LiTaO_3$ over a similar temperature range [16]. This presents a problem for those seeking to fine-tune the VTE process and tightly control the intrinsic defect concentration in $LiTaO_3$. The current work introduces a lower-temperature lithium infiltration anneal (VTI) that is designed to establish a lithium gradient within the treated sample. In this new VTI process, the $LiTaO_3$ crystals are fully buried in a $LiTaO_3$ + Li_3TaO_4 powder that acts as a Li_2O source during the VTI step. This allows partial lithiation to be more observable via measurements of Curie temperature (T_C) and confocal Raman spectroscopy. The VTI thermal treatment is then followed by a high-temperature equilibration anneal lacking any additional lithium sources. Lithium diffusion coefficients in this material are estimated by application of a modified, unrestricted error function or an error function that is constrained by strict boundary conditions to confocal Raman spectroscopy profiles, and the results closely agree with the previous work from Carruthers *et. al.*, who estimated diffusion coefficients by measuring changes in refractive index [16].

Materials and methods

Z-cut single crystals of congruent $LiTaO_3$ (CLT), 10 × 10 × 0.5 mm, were purchased from MTI Corp. Curie temperatures (T_C) of the as-received crystals were confirmed to be ~597 °C via temperature-dependent impedance measurements using painted silver electrodes and an HP 4294A impedance analyzer with 500 mV oscillator from 1 kHz to 1 MHz. These specimens were heated and cooled at a rate of 2 °C/min under ambient atmospheric conditions and a short-circuit configuration. Only the cooling data are reported here.

The crystals were VTI treated in an enclosed platinum crucible and fully buried in a two-phase, reacted powder comprising 62 mol% $LiTaO_3$ and 38 mol% Li_3TaO_4 as a lithium oxide vapor source. The Pt crucible and contents were heated to temperatures between 950 and 1100 °C at a rate of 5 °C/min and soaked for between 15 and 30 hours. After cooling to room temperature at 2 °C/min, the crystals were sectioned, and one half of each crystal was used for T_C and Raman measurements of the chemically graded specimen, while the other half was placed back into a furnace for an equilibration anneal in an ambient atmosphere without the presence of excess lithium oxide. These equilibration anneals varied in duration from twelve to twenty-five hours, but all took place at 1350 °C.

Observation of extremely broad or multiple peaks in the post-equilibration anneal impedance data near the known Curie temperatures of both CLT and stoichiometric $LiTaO_3$ (SLT) was interpreted as indications of retained compositional heterogeneity, requiring the sample to undergo additional thermal treatment to achieve homogeneous Li distribution.

Confocal Raman spectroscopy was performed using a WiTec alpha300 R instrument outfitted with a 532 nm incident laser in $Z(XY)\overline{Z}$ backscatter $^{-}$ configuration to estimate the stoichiometry profile through the bulk of the single crystals. This was accomplished by stepping the height of the optical lens in 5 μm increments and comparing the measured intensity ratio of the Raman mode associated with the intrinsic defects at each step to that of the unaffected A_1(4LO) mode. The confocal optics that the vibrational signal from the samples passes through allow the thickness of the focal layer to be reduced to one micron.

Results and discussion

Indirect stoichiometry analysis for the VTI-treated and air-equilibrated $LiTaO_3$ was carried out via temperature-dependent impedance measurements to identify the Curie temperature of these samples. Figure 1a gives the T_C values for the commercially acquired CLT and SLT crystals, measured at 597 and 697 °C, respectively. These curves are sharp and centered near the temperatures that are well associated with their compositions [17]. Figure 1b shows the effect of the low-temperature VTI anneals on the temperature-dependent permittivity of the originally CLT specimens. In this figure, blue (triangles and dashed) lines represent a specimen that underwent VTI at 950 °C for 15 hours, red (squares and dotted) lines represent a specimen VTI treated at 1000 °C for 10 hours, and black (circles and solid) lines represent a specimen VTI treated at 1050 °C for 10 hours. Each sample that is shown in this figure exhibits two Curie temperature peaks, one at ~ 601 °C and the other at ~ 701 °C, the typical temperatures associated with congruent and stoichiometric $LiTaO_3$ chemistries. The ε′ curves in Fig. 1b exhibit two peaks with a valley at 701 °C, while the ε′′ traces show a single peak at the same temperature. The high conduction current leads to massive uncertainties in the phase angle reported by the LCR meter and thus ambiguity in the assignment of real versus imaginary components. Thus, we use the point where the local extrema align (i.e., valley minimum for ε′ and peak for ε′′) to indicate the temperature of the phase transition. The positions of the two apparent Curie temperatures indicate that both SLT and CLT chemistries are present within these specimens after the VTI treatments. Additionally, the relative permittivity peaks of the VTI specimens are much broader than the peaks of the homogeneous commercial specimens whose chemistries lie at the congruent and stoichiometric points, which would seem to corroborate a broad chemical gradient in the VTI-treated specimens that spans these distinct stoichiometry regions. The real and imaginary permittivity data sharpen considerably after the samples were annealed under ambient conditions and trend toward a single peak that is characteristic of the overall chemistry of the sample. The data in Figure 1c, whose coloring and symbol scheme follows directly from Figure 1b to indicate the parameters for VTI, show the relative permittivity profiles from those selfsame samples after ambient atmosphere equilibration anneals at 1350 °C for 25 hours (blue triangles and dashed line), 12 hours (red squares and dotted line), and 12 hours (black circles and solid line). Cases such as those shown in Figure 1b, where the post-equilibration permittivity data have not yet converged to a single temperature, imply that additional annealing time is required to fully remove the chemical gradient within these samples. In Figure 1c, the real permittivity data denoted by the blue triangles were multiplied by 10x in Figure 1c to better visually distinguish that curve from the other datasets.

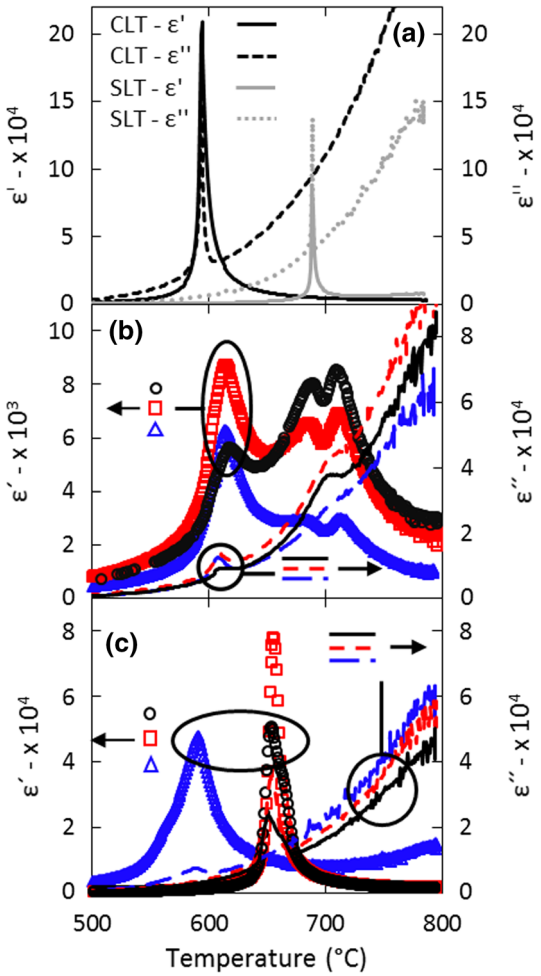

Figure 1 Curie temperature measurements for $LiTaO_3$. **a** Real and imaginary relative permittivity, ε′ and ε′′, respectively, of untreated CLT and commercially VTE annealed SLT. **b** Permittivities of specimens immediately after VTI treatment. **c** ε′ and ε′′ for the same specimens from (**b**) after undergoing equilibration annealing at 1350 °C.

Although these data indicate that there is a spread in lithium concentration within these samples,

impedance spectroscopy alone cannot quantify the stoichiometry gradient magnitude or depth or attempt to measure lithium diffusion in $LiTaO_3$. The equilibration step, in removing the point defect/cation gradient, qualitatively reduces stress gradients within the VTI crystals, observable from a nearly 100% survival rate compared to traditional VTE and Li-rich, nearly stoichiometric crystal growth from melts.

The profile of the cation gradient in the VTI-treated samples was measured via Raman spectroscopy. An example of data from a confocal Raman scan is shown in Figure 2, where the focal plane of the Raman measurement was lowered in 5 μm steps from the surface of the crystal to approximately one half of the full thickness of the specimen. The signal-to-noise ratio decreased rapidly at depths beyond ~200 μm regardless of sample or annealing history, so we focus our Raman analysis on the outer 200 μm of each specimen, which is sufficient for confirming the depth of lithiation in these samples. Each Raman spectrum was normalized to the intensity of the A_1(4LO) band at ~862 cm^{-1}. The relative intensity of the defect-associated peak at ~748 cm^{-1} to the A_1(4LO) peak is known to correlate with Li stoichiometry [18], and Figure 3 plots this relationship across a subset of the VTI conditions studied here.

Figure 3a, b contains compilations of intensity ratio data of the two targeted Raman peaks for samples that underwent VTI at varying times and temperatures. In both plots, the signal ratio is lowest within the top 15 μm of the surface of these samples with an asymptotic rise over 30 to 80 microns to a background level indicative of an unlithiated bulk. While this measurement does not directly quantify Li content, it has been shown previously that mass transport of Li in this system stops when the Li_2O concentration reaches 50.5 mol% [19, 20]. For all samples that were VTI treated at a given temperature, an increase in VTI time appears to increase the lithium concentration at the surface as well as increase the thickness of the lithium-rich surface layer, as expected from classical applications of Fick's laws [21]. This is demonstrated in Fig. 3a by a dataset from samples VTI treated at 950 °C. Increasing the temperature of the VTI treatment has a similar effect, reducing the defect peak intensity and increasing the depth of the lithiated surface layer as shown in Fig. 3b. A Raman profile of a commercially VTE-treated $LiTaO_3$ wafer (Crystal Technology, Inc., VTE parameters unknown, Li/Ta ~0:994) has been added to these plots to provide a reference frame to the in-house treated specimens and shows that even a nearly fully stoichiometric specimen retains measurable amounts of V_{Li}' and Ta_{Li}'''' defect complexes.

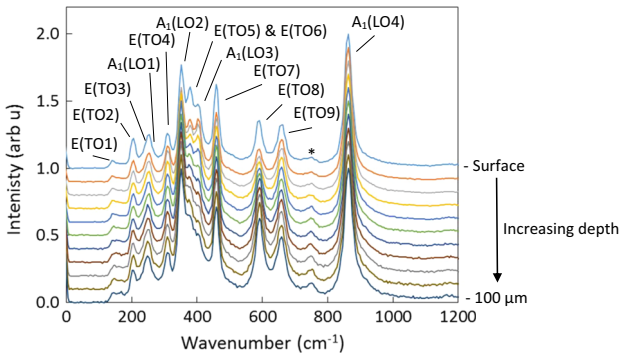

Figure 2 Confocal Raman data from a depth profile down the *c*-axis of a VTE-treated $LiTaO_3$ crystal. Only half the scans from the complete depth profile are shown to prevent data crowding, in addition to shifting the data vertically for clarity. The known Stokes modes are labelled above, and one of the primary extraneous modes that develop with the presence of intrinsic point defects is highlighted by the asterisk.

The samples that are shown in Fig. 3b were subjected to additional annealing, as detailed in the figure caption, in an ambient atmosphere that did not contain excess Li_2O at 1350 °C. Raman data collected after these secondary anneals are shown in Fig. 3c–e. According to these data, the equilibration heat treatments provide sufficient energy to smooth the cation gradient and distribute the lithium that was built up in the surface of the VTI crystals, establishing a more uniform point defect population throughout the bulk of the specimens.

The partial lithium pickup from these lower-temperature VTI anneals established measurable point defect profiles that were mapped with confocal Raman spectroscopy. Reduction of the intrinsic point defect complexes of non-stoichiometric $LiTaO_3$ allows us to track a lithium concentration profile and thus determine lithium diffusion coefficients from the Raman data.

Diffusion coefficients for lithium were calculated from the point defect profiles provided by the Raman data by fitting them with a modified error function (equation 1). Use of the error function necessitates certain assumptions about the diffusion conditions of this study, namely that the system consists of two semi-infinite bodies, that diffusion is constant, and

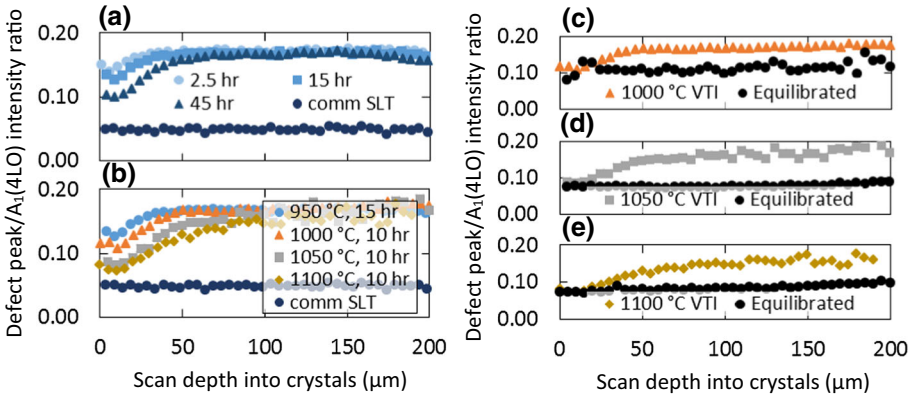

Figure 3 Intensity ratios for the Raman peak associated with intrinsic defect concentration vs. the $A_1(4LO)$ mode plotted as a function focal depth into VTI-treated $LiTaO_3$ single crystals. **a** Signal versus depth profiles of different samples VTI treated at 950 °C for 2.5, 15, and 45 hours. **b** A comparison of many specimens VTI treated at different times and temperatures. Data from a commercial VTE-treated stoichiometric crystal are featured for comparison to show that a nonzero signal is detectable in approximately fully lithiated $LiTaO_3$. **c**–**e** Comparisons between the samples from 3b (color based on VTI treatments listed in plot **b**) and their counterparts after having undergone the equilibrium annealing process to homogenize crystal chemistry (black) for 12, 10, and 10 hours (**c**–**e**, respectively).

that diffusion is only occurring during the soak step of VTI and not on heating or cooling.

$$c(x,t) = A + Berf\left(\frac{x+y}{\sqrt{4Dt}}\right) \quad (1)$$

In equation 1, $c(x, t)$ is lithium concentration as a function of position in the sample and duration of VTE treatment, A and B are unitless constants, x is depth into the sample, y is an offset factor to x that shifts the inflection point of the error function to the proper location within the relithiated surface layer to compensate for the potential of an increasing thickness of a fully lithium-saturated region of $LiTaO_3$, D is the diffusion coefficient, and t is the duration of the VTE treatment. This equation is not bound by any starting or final chemical information, so another calculation with a slightly more structured set of boundary conditions was utilized to confirm the coefficients indicated by equation 1.

Application of chemical information gained from T_C data after VTI and equilibration anneals and the depth at which the Raman data returned to nominally congruent levels post-VTE provided the chemical and physical boundary conditions that were used to confirm the results found with the unbounded equation 1. Equation 2 is structured as follows:

$$c(x,t) = c_i + (c_s - c_i)erfc\left(\frac{x+y}{\sqrt{4Dt}}\right) \quad (2)$$

where c_i represents the initial chemistry of the crystal, i.e., congruent, and c_s is the chemistry of the lithiated surface layer of the specimen as determined by the best fit of the Raman profile considering an upper limit of 50.5 mol% Li_2O due to the thermodynamic termination of any mass transfer due to VTE. The resulting diffusion coefficients for lithium in $LiTaO_3$ are displayed in Figure 4. Reports for similar diffusion coefficients are available in the literature for lithium niobate but are largely lacking for lithium tantalate. Manually applying the chemical boundary information into the error function equations does not appear to have significantly impacted the diffusion coefficients calculated in this work, as the

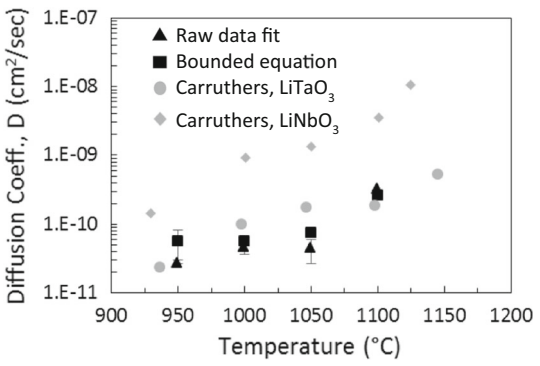

Figure 4 Diffusion coefficients for lithium in VTE-treated $LiTaO_3$ calculated from Raman and Curie temperature data and compared to literature values for $LiTaO_3$ and $LiNbO_3$ along the polar axis.

coefficients differ by less than 3.5×10^{-10} cm^2/s at all investigated temperatures, adding confidence to the conclusions. The mean lithium diffusion coefficients found at 950 °C and 1100 °C are 4.2×10^{-11} cm^2/s and 2.9×10^{-10} cm^2/s, respectively. Data on lithium out-diffusion in $LiTaO_3$ as a function of temperature, from Carruthers et al. [16], remain within an order of magnitude of our data and suggest that surface adsorption and desorption reactions are not rate-limiting steps in lithium gain or loss during the VTI and VTE processes. Figure 4 also features lithium diffusion coefficients in $LiNbO_3$ for visual reference. All of the coefficients being reported for $LiTaO_3$ are noticeably lower than those for $LiNbO_3$, though this phenomenon is not unexpected given that the lattice of lithium niobate is likely to be much softer than that of $LiTaO_3$ at these temperatures due to the relative proximity to the melting point [22–26].

Locating the Matano plane through a Boltzmann–Matano analysis to ensure that the integrated areas bound by the diffusion profile are equal on both the surface and crystal-bulk sides of the concentration curve would be one method to increase the accuracy of the diffusion coefficients calculated here. Additionally, full consideration of ambipolar diffusion principles to account for tantalum diffusion in concert with lithium would be prudent for a more complete discussion of multi-species diffusion in $LiTaO_3$.

Conclusions

Low-temperature vapor transport infiltration was used to develop a lithium concentration gradient in lithium tantalate single crystals, which was later removed through a chemistry-equilibrating and stress-reducing anneal in ambient atmosphere. Lithium concentration profiles were inferred from confocal Raman spectroscopy measurements of point defect concentration, and diffusion coefficients of $\sim 4.2 \times 10^{-11}$ to $\sim 2.9 \times 10^{-10}$ cm^2/s were calculated for lithium in $LiTaO_3$ between 950 and 1100 °C. Curie temperature values determined by permittivity measurements suggest that these conditions achieve a nearly stoichiometric composition within the outer ~ 15 μm of the single crystals, and that, as vapor transport infiltration temperature increases, lithium concentrations decrease to CLT levels at increasing distances from the crystal surface, ranging between 30 and 80 μm.

Acknowledgements

Jacob M. Ivy and Geoff L. Brennecka were supported in part by the National Science Foundation under Grant No. DMR-1555015.

Declarations

Conflict of interest The authors declare that they have no conflict of interest that could potentially influence or bias this work.

References

[1] Kim S, Gopalan V, Kitamura K, Furukawa Y (2001) Domain reversal and nonstoichiometry in lithium tantalate. J Appl Phys 90(6):2949–2963. https://doi.org/10.1063/1.1389525

[2] Hum DS, Route RK, Miller GD, Kondilenko V et al (2007) Optical properties and ferroelectric engineering of vapor-transport-equilibrated, near-stoichiometric lithium tantalate for frequency conversion. J Appl Phys 101:093108. https://doi.org/10.1063/1.2723867

[3] Shur VY, Akhmatkhanov AR, Baturin IS, Shishkina EV (2012) Polarization reversal and jump-like domain wall motion in stoichiometric $LiTaO_3$ produced by vapor transport equilibration. J Appl Phys 111:014101. https://doi.org/10.1063/1.3673601

[4] Jazbinšek M, Zgonik M, Takekawa S, Nakamura M, Kitamura K, Hatano H (2002) Reduced space-charge fields in near-stoichiometric $LiTaO_3$ for blue, violet, and near-ultraviolet light beams. Appl Phys B Lasers Opt 75(8):891–894. https://doi.org/10.1007/s00340-002-1069-3

[5] Kitamura K, Furukawa Y, Takekawa S, Hatanaka T, Ito H, Gopalan V (2001) Non-stoichiometric control of $LiNbO_3$ and $LiTaO_3$ in ferroelectric domain engineering for optical devices. Ferroelectrics 257:235–243. https://doi.org/10.1080/00150190108016305

[6] Kitamura K, Furukawa Y, Niwa K, Gopalan V, Mitchell TE (1998) Crystal growth and low coercive field 180° domain switching characteristics of stoichiometric $LiTaO_3$. Appl Phys Lett 73(21):3073–3075. https://doi.org/10.1063/1.122676

[7] Gopalan V, Mitchell TE, Furukawa Y, Kitamura K (1998) The role of nonstoichiometry in 180° domain switching of $LiNbO_3$ crystals. Appl Phys Lett 72(16):1981–1983. https://doi.org/10.1063/1.121491

[8] Kitamura K, Yamamoto JK, Iyi N, Kimura S, Hayashi T (1992) Stoichiometric $LiNbO_3$ single crystal growth by double crucible Czochralski method using automatic powder supply system. J Cryst Growth 116:327–332. https://doi.org/10.1016/0022-0248(92)90640-5

[9] Tian L, Gopalan V, Galambos L (2004) Domain reversal in stoichiometric $LiTaO_3$ prepared by vapor transport equilibration. Appl Phys Lett 85(19):4445–4447. https://doi.org/10.1063/1.1814436

[10] Bordui PF, Norwood RG, Bird CG, Carella JT (1995) Stoichiometry issues in single-crystal lithium tantalate. J Appl Phys 78:4647–4650. https://doi.org/10.1063/1.359811

[11] Kostritskii SM, Aillerie M, Bourson P, Kip D (2009) Raman spectroscopy study of compositional inhomogeneity in lithium tantalate crystals. Appl Phys B 95:125–130. https://doi.org/10.1007/s00340-009-3442-y

[12] Fontana MD, Bourson P (2015) Microstructure and defects probed by Raman spectroscopy in lithium niobate crystals and devices. Appl Phys Rev 2:040602. https://doi.org/10.1063/1.4934203

[13] Shi L, Kong Y, Yan W, Liu H et al (2005) The composition dependence and new assignment of the Raman spectrum in lithium tantalate. Solid State Commun 135:251–256. https://doi.org/10.1016/j.ssc.2005.04.024

[14] Bordui PF, Norwood RG, Jundt DH, Fejer MM (1992) Preparation and characterization of off-congruent lithium niobate crystal. J Appl Phys 71(2):875–879. https://doi.org/10.1063/1.351308

[15] Bäumer C, David C, Tunyagi A, Betzler K, Hesse H, Krätzig E, Wöhlecke M (2003) Composition dependence of the ultraviolet absorption edge in lithium tantalate. J Appl Phys 93(5):3102–3104. https://doi.org/10.1063/1.1542689

[16] Carruthers JR, Kaminow IP, Stulz LW (1974) Diffusion kinetics and optical waveguiding properties of outdiffused layers in lithium niobate and lithium tantalate. Appl Opt 13(10):2333–2342. https://doi.org/10.1364/ao.13.002333

[17] Gopalan V, Dierolf V, Scrymgeour DA (2007) Defect—domain wall interactions in trigonal ferroelectrics. Annu Rev Mater Res 37:449–489. https://doi.org/10.1146/annurev.matsci.37.052506.084247

[18] Kostritskii SM, Bourson P, Aillerie M, Fontana MD, Kip D (2006) Quantitative evaluation of the electro-optic effect and second-order optical nonlinearity of lithium tantalate crystals of different compositions using Raman and infrared spectroscopy. Appl Phys B Lasers Opt 82:423–430. https://doi.org/10.1007/s00340-005-2046-4

[19] Nassau K, Lines ME (1970) Stacking-fault model for stoichiometry deviations in $LiNbO_3$ and $LiTaO_3$ and the effect on the curie temperature. J Appl Phys 41(2):533–537. https://doi.org/10.1063/1.1658708

[20] Hum D (2007) Frequency conversion in near-stoichiometric lithium tantalate fabricated by vapor transport equilibration. Ph.D. dissertation, Stanford University

[21] Balluffi RW, Allen SM, Carter WC (2005) Kinetics of materials, 1st edn. John Wiley & Sons Inc, New Jersey

[22] Li Q, Sun J, Yang J, Shang J, Zhang L, Xu J (2016) Lithium diffusion in lithium niobate crystals with different initial Li_2O content at high temperature. J Am Ceram Soc 99(9):3055–3059. https://doi.org/10.1111/jace.14329

[23] Jundt DH, Fejer MM, Norwood RG, Bordui PF (1992) Composition dependence of lithium diffusivity in lithium niobate at high temperature. J Appl Phys 72(8):3468–3473. https://doi.org/10.1063/1.351422

[24] Zhang DL, Zhang WJ, Zhuang YR, Pun EYB (2007) Dynamic simulation of vapor transport equilibration in congruent $LiNbO_3$ crysta. Cryst Growth Des 7(8):1541–1546. https://doi.org/10.1021/cg0605685

[25] Chen B, Hua PR, Zhang DL, Pun EYB (2012) Stoichiometry dependence of Li^+ diffusivity in $LiNbO_3$ crystal in off-congruent, Li-deficient regime. J Am Ceram Soc 95(3):1018–1022. https://doi.org/10.1111/j.1551-2916.2011.04906.x

[26] Chin GY, Ballman AA, Tien PK, Riva-Sanseverino S (1975) Diffusion kinetics and optical quality in $LiNbO_3$-$LiTaO_3$ optical waveguides. Appl Phys Lett 26(11):637–639. https://doi.org/10.1063/1.88008